Numerical Investigation of the Dynamics of a Flexible Filament in the Wake of Cylinder

Ru-Nan Hua[1], Luoding Zhu[2] and Xi-Yun Lu[1,*]

[1] *Department of Modern Mechanics, University of Science and Technology of China, Hefei 230026, China*
[2] *Department of Mathematical Sciences, Indiana University-Purdue University Indianapolis, 402 North Blackford Street, Indianapolis, IN 46202, USA*

Abstract. Fluid-structure-interaction problems are ubiquitous, complicated, and not yet well understood. In this paper we investigate the interaction of a leading rigid circular cylinder and a trailing compliant filament and analyze the dynamic responses of the filament in the wake of the cylinder. It is revealed that there exist two flapping states of the filament depending on the cylinder-filament separation distance and the relevant critical distance distinguishing the two states is associated with the Reynolds number and the filament length. It is also found that the drag coefficient of the cylinder is reduced but that of the filament may be increased or decreased depending on its length. Compared with a single filament in a uniform flow, the filament of the same mechanical properties flapping in the wake of the cylinder has a lower frequency and a greater amplitude.

AMS subject classifications: 74K20, 76D05, 76Z10

Key words: Fluid-structure interaction, immersed boundary-lattice Boltzmann method.

1 Introduction

Fluid-structure-interaction (FSI) problems are everywhere in our daily life. Arguably the FSI problems may be further categorized into two subsets: fluid-*rigid*-structure-interaction such as a flying aircraft interacting with the air and fluid-*flexible*-structure-interaction such as red blood cells moving in the flowing blood in human arteries. These two types of the FSI problems have already been extensively studied theoretically, experimentally and computationally. The readers are referred to the following papers and

---

*Corresponding author.
URL: http://staff.ustc.edu.cn/~xlu/
Email: xlu@ustc.edu.cn (X. Y. Lu)

references therein: sedimentation of an elliptical particle [1], numerical simulations on the dynamics of plates falling freely in a fluid under the influence of gravity [2]; experimental and computational studies on the dynamics of flexible filaments in a flowing soap film [3,4], a flapping flexible plate in quiescent fluid [5], resonance and propulsion performance of a heaving flexible wing [6], capsule deformation [7,8], and effects of flexibility on the aerodynamic performance of flapping wings [9].

However, many FSI problems encountered are even more complicated. They may involve the interaction of a viscous fluid and both rigid and flexible structures. To name a few such examples: flag flapping in a wind (involving the rigid pole, the flexible flag and the flowing air) and fish swimming in the wake of a bridge pillar or a navigating ship. The FSI problems involving both rigid and compliant structures in a viscous flow are less investigated and yet not well understood because of the intrinsic mathematical and physical complexity of this type of fluid-structure-interaction. Liao et al. [10] demonstrated how a trout might exploit the vortices to reduce the cost of locomotion in the wake of a stationary object in a water flow. Beal et al. [11] showed that a streamlined body passively oscillating within a vortical wake could extract sufficient energy from the eddies to propel itself upstream. Eldredge and Pisani [12] investigated the passive locomotion of a simple articulated fish-like system in the wake of an obstacle. Sui et al. [13] first simulated the interaction of a leading rigid cylinder and a trailing *massless* flexible filament in a two-dimensional flow as application of a newly developed numerical method for the FSI problems. Jia and Yin [14] identified by laboratory experiments three response modes of a flexible filament in the wake of a rigid cylinder in a flowing soap film. Wang et al. [15] found the filament in the wake of a upperstream cylinder gained a thrust rather than drag in two dimensions. Tian et al. [16] performed simulations on the interaction of a leading flexible filament and a trailing rigid cylinder.

Because of the presence of both rigid and deformable bodies in a viscous flow, the interaction among the bodies and the flow may become different and more complex, and new phenomena may emerge. Previous experiments with tandem rigid cylinders [17] found that the drag of a trailing object was less than that of a leading one. A recent experiment on two tandem flapping rubber threads in a two-dimensional viscous flow reported by Ristroph and Zhang [18] revealed just the opposite: the drag of the downstream flag was greater than that of the upstream flag. A computational study [19] on the similar problem showed that even more complicated scenarios happened as the Reynolds number was varied. What would happen if a rigid body and a deformable body are placed in tandem in a viscous flow? Here we consider a flexible filament interacting with the wake of a upstream rigid cylinder in a viscous incompressible flow in two dimensions. Numerous simulations are performed with various dimensionless parameters and our numerical results indicate the existence of two flapping modes of the filaments associated with the suction zone behind the cylinder [12] and the drag of the leading cylinder is always reduced but the drag of the trailing filament may be decreased or increased depending on the dimensionless filament length.

The remainder of the paper is organized as follows. Section 2 presents the physical

problem and the relevant mathematical description. Section 3 briefly outlines the numerical methods. Section 4 addresses the simulation results in detail with discussions. Finally a brief summary concludes the present work.

2   Physical problem and mathematical formulation

We consider a viscous flow past a rigid circular cylinder of diameter D and a flexible filament of length L which is introduced behind the cylinder with one end pinned and otherwise unrestricted. As shown in Fig. 1, the extent of space between the filament fixed-end and the cylinder center is $0.5D+G$ in the horizontal direction and H in the vertical direction. This problem is representative of the fluid-structure-interaction that involves a fixed rigid structure, a movable compliant structure with one end constraint and a viscous incompressible fluid. The motion of the fluid can be described by the viscous incompressible Navier-Stokes equations

$$\frac{\partial v}{\partial t}+v\cdot\nabla v=-\frac{1}{\rho}\nabla p+\frac{\mu}{\rho}\nabla^2 v, \tag{2.1a}$$

$$\nabla\cdot v=0, \tag{2.1b}$$

where v is the velocity, p the pressure, ρ the density of the fluid and μ the fluid dynamic viscosity.
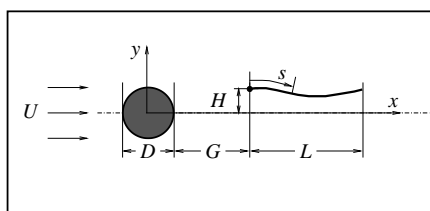

Figure 1: Sketch of the problem of a flapping filament in the wake of a circular cylinder in a uniform incoming flow. The cylinder is fixed and the filament is pinned at the fixed-end marked by a small solid circle.

The boundary conditions are as follows

$$v=(U,0), \tag{2.2}$$

on the inlet, top and bottom boundaries, where U represents the free-stream velocity,

$$\frac{\partial v}{\partial x}=0, \quad \frac{\partial p}{\partial x}=0, \tag{2.3}$$

on the outlet, and

$$v=0, \tag{2.4}$$

on the cylinder.

The initial condition is as follows

$$v = (U, 0),$$ (2.5)

on the flow domain.

The dynamics of the filament can be governed by the following equation

$$\rho_l \frac{\partial^2 X}{\partial t^2} - \frac{\partial}{\partial s}\left[T(s)\frac{\partial X}{\partial s}\right] + EI\frac{\partial^4 X}{\partial s^4} = F,$$ (2.6)

with s as the Lagrangian coordinate along the length, and the body position vector $X(s, t)$. Here, ρ_l is the structural linear density, $T(s) = Eh(|\partial X/\partial s| - 1)$ is the tension, Eh is the coefficient of stretching and compression, EI is the structural bending rigidity, and F is the load of fluid.

The boundary conditions for the filament are

$$X(s=0,t) = (x_0, y_0), \quad \frac{\partial^2 X}{\partial s^2}(s=0,t) = (0,0),$$ (2.7)

at the fixed end ($s=0$), where $(x_0, y_0) = (0.5D + G, H)$ is its coordinates, and

$$T(s=L,t) = 0, \quad \frac{\partial^2 X}{\partial s^2}(s=L,t) = (0,0), \quad \frac{\partial^3 X}{\partial s^3}(s=L,t) = (0,0),$$ (2.8)

at the free end ($s=L$). The velocity of the filament is

$$v = \frac{\partial X}{\partial t}.$$ (2.9)

The initial condition is

$$X(s,t=0) = (x_0 + s, y_0), \quad \frac{\partial X}{\partial t}(s,t=0) = (0,0).$$ (2.10)

We choose ρ, U, and D as reference quantities to non-dimensionalize the above equations. Based on the non-dimensional analysis, there exist several dimensionless parameters in our problem: the Reynolds number $Re = \rho U D/\mu$, the stretching coefficient $K_s = Eh/(\rho U^2 D)$, the bending coefficient $K_b = EI/(\rho U^2 D^3)$, the linear density ratio $M = \rho_l/(\rho D)$, the length of the filament L/D, the horizontal gap between the cylinder and the filament fixed-end G/D, and the vertical distance of the fixed-end to the centerline H/D. The time t, the frequency f and the drag C_D are non-dimensionalized by D/U, U/D and $1/2\rho U^2 D$, respectively. In the remainder of the paper, we use L, G, and H to represent L/D, G/D, and H/D respectively for simplicity of notation and all variables and their cited values are dimensionless.

3 Numerical method

The governing equations given above are solved numerically using a modified penalty immersed boundary method coupled with a lattice Boltzmann method which was described in detail in [20]. A brief description of the method is only provided here.

The Navier-Stokes equations are approximated by the discrete lattice-Boltzmann equation with a single relaxation time D2Q9 model, and the multi-block method [21] is employed to improve the computational efficiency. The fluid-cylinder-filament interaction is handled by a modified version of the penalty immersed-boundary method originally developed by Kim and Peskin [22]. In this method, the no-slip boundary condition (on the filament and on the cylinder surface) is achieved by including a body force density $f(x,t)$ into the right hand side of the momentum Eq. (2.1) which is defined as follows

$$f(x,t) = \int_\Gamma F(s,t)\delta(x - X(s,t))\mathrm{d}s, \qquad (3.1)$$

where $F(s,t)$ represents the interaction force between the fluid and the structures (including the filament and cylinder), and $\delta(x - X(s,t))$ is Dirac delta function. The velocity of the filament is interpolated from the flow field onto the Lagrangian points discretizing the filament, and the positions of those points are updated by explicitly integrating the velocity in Eq. (2.9). The last two terms on the left hand side of Eq. (2.6) are calculated explicitly by finite-difference method [4]. To calculate the first term (i.e., inertial force term) in Eq. (2.6), the penalty method used in [22] is adopted to ensure the numerical stability. Specifically, the filament itself is assumed to be massless in the algorithm, but a ghost filament of linear density ρ_l is attached to the physical filament through a series of virtual spring of specified stiffness. The inertial force term in Eq. (2.6) is thus replaced by the virtual-spring force. A direct forcing method [13,23] is employed to calculate the interacting force between the cylinder and the fluid. The method and the code used for our current study have been validated carefully in our previous papers [16,20,24].

4 Results and discussion

In the present simulations, the computational domain for fluid flow is chosen as $-10 \le x \le 30$ and $-10 \le y \le 10$ based on our computational examinations. Two level multi-blocks are employed, with the fine lattice spacing of 0.02 near the region of the cylinder and filament and the coarse lattice spacing of 0.04 away from these immersed boundaries.

For most of the simulations discussed in this paper, an elastic homogeneous massive filament with invariant mechanical properties is considered. The stretching coefficient, bending coefficient, and linear density ratio of the filament are constant: $K_s = 1000$, $K_b = 0.0001$, $M = 0.3$. The Reynolds number of the flow is $Re = 100$ unless otherwise stated. The choice of the value of K_s makes sure that the filament extension is small. Note that at these values of Re and M an isolated filament without the cylinder in a

uniform flow settles down to a period-one limit-cycle oscillation of constant frequency and amplitude [25]. The relevant resultant quantities such as drag coefficient of this case will be used for comparison with those of the fluid-cylinder-filament system. There are seven independent dimensionless parameters in this problem, we here focus on simulation results for the parameters in the following ranges: $L = 0.5 - 3.0$, $H = 0.0 - 2.0$ and $G = 1.5 - 15.0$.

4.1 Two flapping modes

First of all, we set $H = 0.0$ to isolate the influence of the horizontal cylinder-filament separation distance G on the motion of the fluid-cylinder-filament system. Extensive simulations are performed with a series of different values of G. Our simulation results reveal an interesting phenomenon: if the filament is placed far enough away from the cylinder, i.e., when G is large enough, the filament flaps in the wake of the cylinder in a way similar to the case where the cylinder is absent, i.e., filament flapping in a uniform flow [4]; however, if the filament is placed close enough to the upstream cylinder, i.e., when G is small enough, the filament reverses its flapping direction–the free-end moves upperstream passing the fixed-end and moving towards the cylinder, and finally settles down to a self-sustained flapping state with the free-end upperstream and the fixed-end downstream. We call the former situation "normal flapping" (NF) and the latter situation "reversed flapping" (RF). To identify the critical horizontal cylinder-filament distance G_c for distinguishing the two types of flapping, a series of simulations with different values of G are performed and the critical value G_c is obtained to be approximately 2.65, as exhibited on the second row of Table 1.

To examine whether the interesting phenomenon is sensitive to the filament initial orientation, i.e., the relative position of fixed-end and free-end with respect to the cylinder, all of the above simulations used to estimate G_c are repeated with only the initial filament orientation changed and all of the parameters remained the same, i.e., filament free-end placed upperstream and the fixed-end downstream. We find that the switch between the normal and reversed flapping is independent of the filament initial orientation. See the results on the third row of Table 1.

To investigate the physical mechanism in the reversed flapping mode, the flow behavior behind the cylinder is analyzed. Usually, a backflow zone is formed in the region behind the cylinder. Such a region where the x-component of velocity is negative is

Table 1: Effect of cylinder-filament separation distance G on flapping modes at $L = 2.0$ and $H = 0.0$ for two different initial orientations of the filament. $\Rightarrow (t = 0)$: filament initially placed with the fixed-end towards the cylinder; $\Leftarrow (t = 0)$: filament initially placed with the free-end towards the cylinder. Normal flapping (NF): the filament flaps with the fixed-end towards the cylinder; reverse flapping (RF): the filament flaps with the the free-end towards the cylinder.

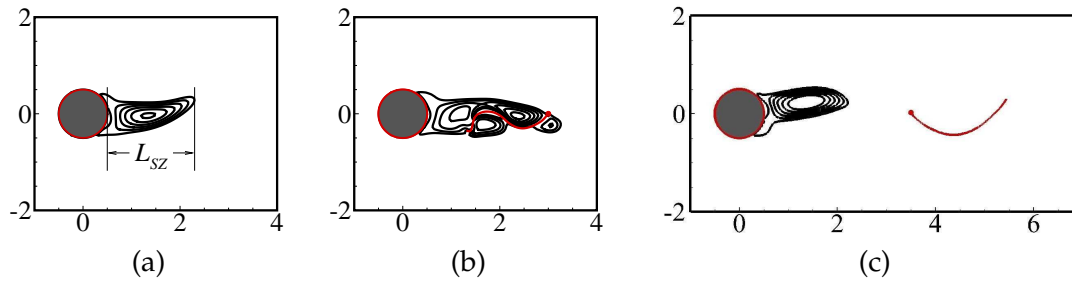| G	1.5	2.0	2.6	2.7	3.5
$\Rightarrow (t = 0)$	RF	RF	RF	NF	NF
$\Leftarrow (t = 0)$	RF	RF	RF	NF	NF

Figure 2: Instantaneous suction zone of (a) an isolated cylinder and filament and cylinder system for $G=$ (b) 2.5 and (c) 3.0, $L=2.0$, and $H=0.0$.

called a suction zone [12], i.e., the region defined by the set $\{(x,y)|u(x,y)<0, x>0$ and $-D/2\leq y\leq D/2\}$ on the x–y plane. In this suction zone the pressure is lower and fluid particles move against the mainstream. Fig. 2(a) shows the shape and size of a typical suction zone behind a cylinder without the filament. Note that the suction zone oscillates up and down with respect to the horizontal line because of vortex shedding from the cylinder. The presence of the suction zone is behind the interesting phenomenon of reversed filament flapping identified by our numerical simulations. Presumably, when the filament is initially placed outside of the suction zone, the normal flapping happens; when it is placed within the suction zone, the reversed flapping happens. However, as seen from Figs. 2(b) and (c), the introduction of a filament behind the cylinder changes the size of the suction zone: the zone is elongated by the flapping filament behind. Thus, the critical separation distance G_c of the two flapping modes may be dependent on other dimensionless parameters of the system that affect the suction zone.

Therefore we further investigate the effect of a couple of important dimensionless

Table 2: Effect of filament length L on the critical gap G_c for $H=0.0$.

L	1.0	1.5	2.0	2.5
G_c	2.25	2.42	2.65	2.82

Table 3: Effect of vertical distance H on the critical gap G_c for $L=2.0$.

H	0.0	0.1	0.2	0.3	0.4	0.5
G_c	2.65	2.62	2.60	2.55	2.45	None

Table 4: Effect of Reynolds number Re on the critical gap G_c for $L=2.0$ and $H=0.0$.

Re	100	200	300
G_c	2.65	2.45	2.05

Table 5: Effect of Reynolds number Re on the mean value of the suction zone length $\bar{L}_{SZ}$ for an isolated cylinder in a uniform flow. The suction zone length L_{SZ} is defined as shown in Fig. 2(a).

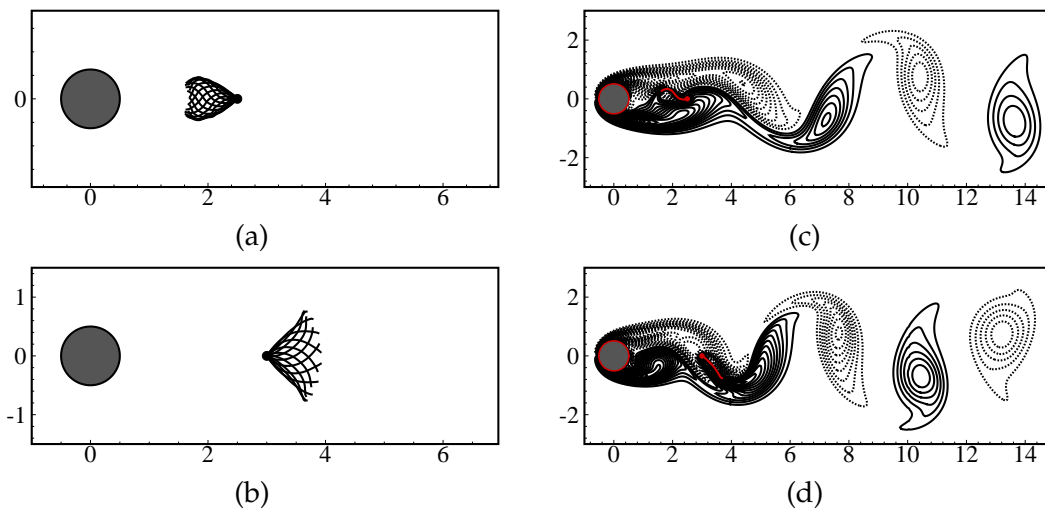| Re	100	200	300
$\bar{L}_{SZ}$	1.8	1.2	1.0

Figure 3: (a), (b) Envelopes of the filament and (c), (d) instantaneous vorticity contours for $L=1.0$, $H=0.0$, and $G=$ (a), (c) 2.0 (RF) and (b), (d) 2.5 (NF).

parameters L, H, and Re on the critical cylinder-filament distance G_c. Table 2 indicates that G_c increases with the filament length. This may be caused by the elongation of the suction zone due to the presence of the filament. A longer filament may induce a greater elongation within certain range and thus increase the critical cylinder-filament separation distance G_c. Table 3 shows that the critical value G_c decreases as vertical distance H increases, and when $H \geq 0.5$ the filament does not have the RF state. The results may be explained by the gradual tapering of the suction zone shape downstream of the cylinder, as seen in Fig. 2. Table 4 shows that the critical value is a decreasing function of the Reynolds number Re. To explain this, several simulations are done to demonstrate the influence of Re on the size of the suction zone. The mean length of the suction zone $\bar{L}_{SZ}$ versus Re is given in Table 5. It is shown that as the Re increases the mean length decreases. Higher Re usually causes higher frequency of vortex shedding and therefore higher frequency of the suction zone oscillation which may cause the breakage of the suction zone and result in shrinkage of the suction zone. Thus higher Re results in shorter mean suction zone length. This may explain the results in Table 4.

Fig. 3 illustrates the envelope of the flapping filament and the vorticity contours of the flow for the filament in NF and RF states for $L=1$. Two major differences between the two flapping states are identified as follows. One is the sign of shed vortices in the wake, and the other is the size of filament flapping envelope. This is caused by the restriction of the suction zone of the cylinder. The suction zone height is less than the cylinder diameter. But the filament in the normal flapping state has no such constraints in the vertical direction, its free-end may go as far as it can vertically. Therefore the filament possesses a wider envelope.

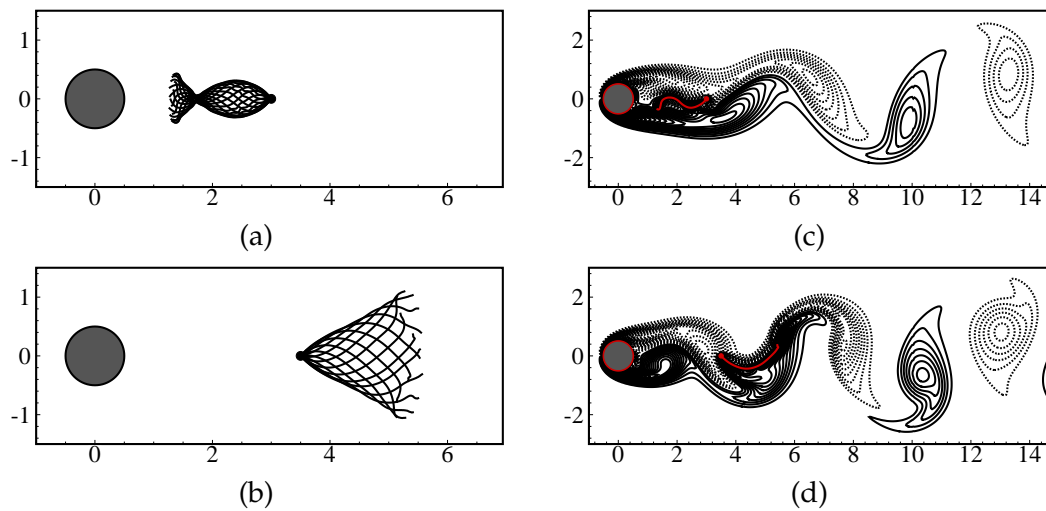Similarly, Figs. 4 and 5 show the envelopes of the flapping filament and the vorticity

Figure 4: (a), (b) Envelopes of the filament and (c), (d) instantaneous vorticity contours for $L=2.0$, $H=0.0$, and $G=$ (a), (c) 2.5 (RF) and (b), (d) 3.0 (NF).
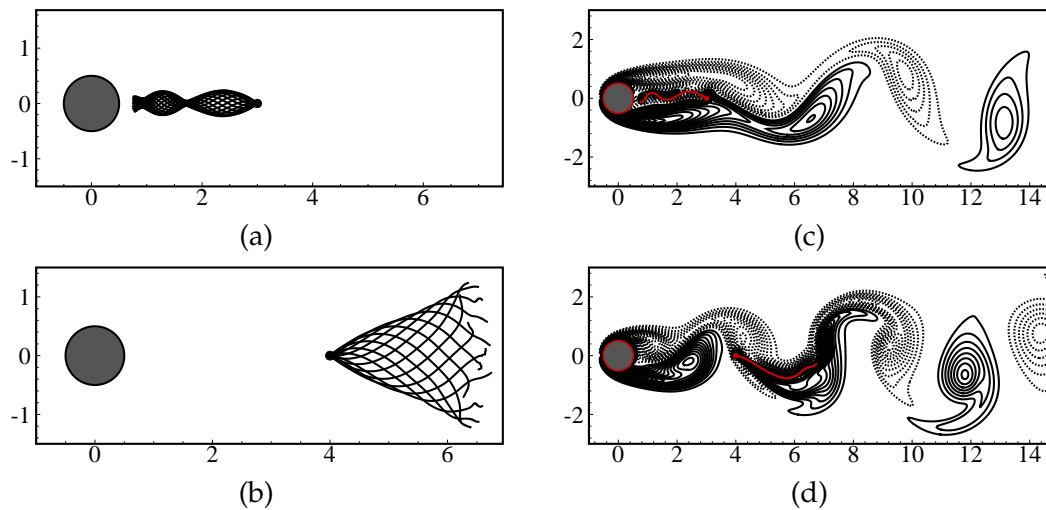

Figure 5: (a), (b) Envelopes of the filament and (c), (d) instantaneous vorticity contours for $L=2.5$, $H=0.0$, and $G=$ (a), (c) 2.5 (RF) and (b), (d) 3.5 (NF).

contours of the flow for the filament in NF and RF states for $L=2.0$ and $L=2.5$, respectively. Compared to the Fig. 3 for $L=1.0$, a striking difference exists in the shape of the envelope of filament in the reversed flapping state: the envelope becomes fish-like for $L=2.0$ and becomes multiple-section-lotus-root like for $L=2.5$. The spindle-like sub-structure of the envelope is caused by the constraint imposed by the limited size of the suction zone on the filament flapping motion. The filament cannot flap beyond the boundary of the suction zone, thus forced to oscillate more frequently with smaller wave

numbers in a narrow space along the vertical direction, thus forming more spindle-like sub-structures. The envelope of the filament at normal flapping state simply gets bigger as L increases since a longer filament sweeps across a bigger area when it flaps.

4.2 Drag coefficients

Previous experimental results on two tandem bodies in a viscous flow revealed that the drag of a trailing body was reduced in the case of two rigid bodies [17] and the drag of the leading body was reduced in the case of two compliant bodies [18]. What would happen in the present case where the leading object is rigid and the trailing object is compliant?

Now let us look at the drag coefficients of the cylinder, the filament and the whole cylinder-filament system. First we report the influence of the horizontal cylinder-filament separation distance on the drag coefficients (i.e., $H=0.0$). Fig. 6 plots the drag coefficients of the cylinder and the filament as functions of the separation distance G for $L=1.0$ and 2.0. These plots show that the C_D of the cylinder is reduced by the presence of the filament; however, the C_D of the filament is length dependent: it is reduced when $L=1.0$ and it is increased when $L=2.0$. It is noticed that there always exists a jump in these functions which corresponds to the critical value of the separation distance G_c. When $G<G_c$, the drag coefficients of both the cylinder and the filament are significantly reduced; when $G>G_c$, the drag coefficients are bounded above by the drag coefficients of the cylinder (without the filament) and filament (without the cylinder) except for the
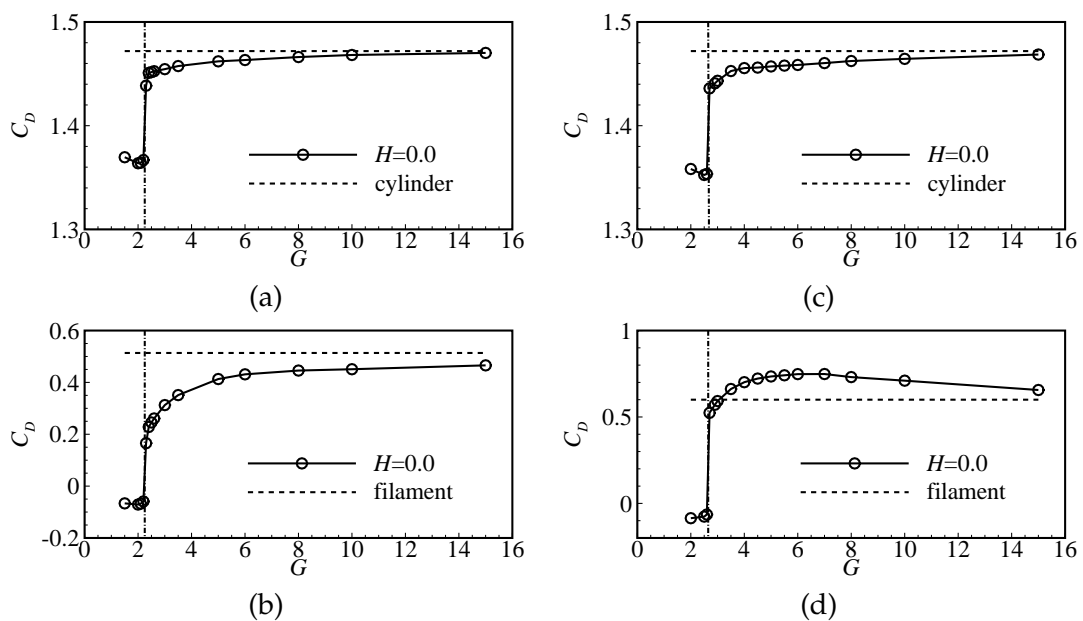

Figure 6: Drag coefficient C_D of the cylinder (a), (c) and the filament (b), (d) versus G for $L=1.0$ (a), (b) and 2.0 (c), (d). In the legends, "cylinder" and "filament" represent the results for the corresponding isolated bodies.
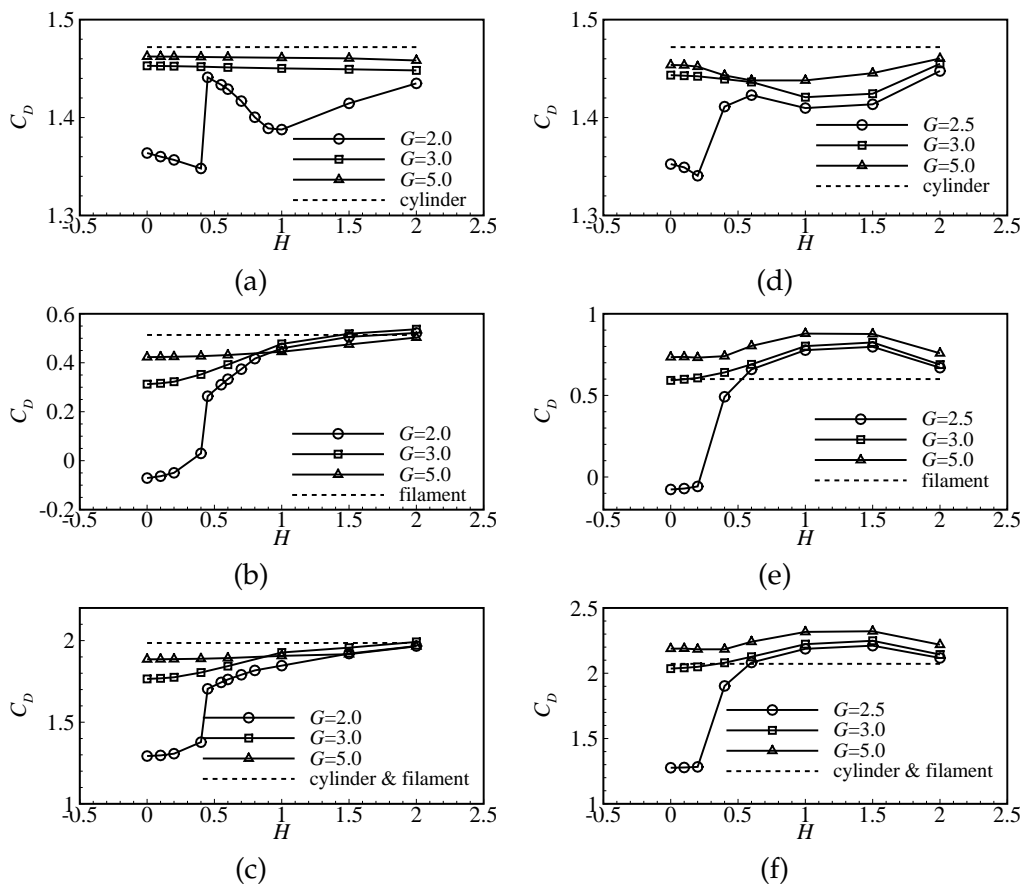
Figure 7: Drag coefficient C_D of the cylinder (a), (d), the filament (b), (e) and the sum of both (c), (f) versus H for $L = 1.0$ (a)-(c) and 2.0 (d)-(f).

$L = 2.0$ case where the drag coefficient of the filament is increased when outside of the suction zone (i.e., $G > G_c$). In either case, the drag coefficients approach the corresponding drag coefficient of the cylinder alone case or the filament alone case, respectively.

Presumably the drag reduction of the cylinder is caused by the trailing flapping filament. The filament in flapping state (NF or RF) acts as a flow stopper/divider that increases the pressure behind the cylinder hence reduces the drag of the cylinder. The longer the filament, the farther the filament free-end may reach out vertically, thus the greater the flapping amplitude. As a consequence, the flapping filament presents as a larger effective object downstream and therefore causes more drag reduction for the upperstream cylinder. This phenomenon has also been found for the rigid plate splitter in the wake of cylinder [26]. This is the reason why the cylinder drag coefficient decreases with the filament length. When the filament is short, it flaps in the vicinity of the cylinder and the pressure near the fixed-end is less compared to the uniform coming flow, thus the drag is reduced. When the filament is longer, the pressure near the free-end is greater
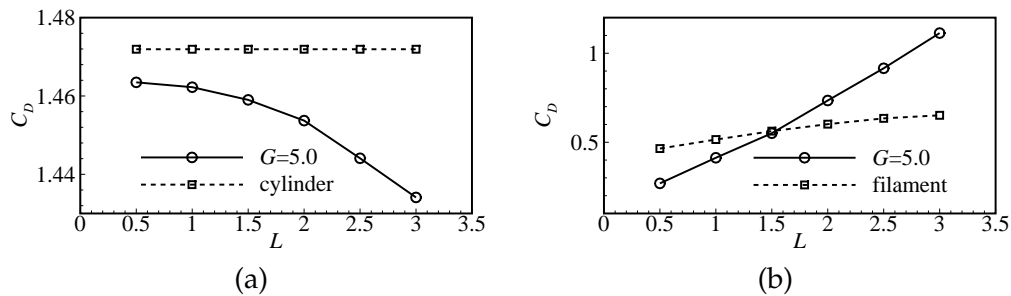
Figure 8: Drag coefficient C_D of the cylinder (a) and the filament (b) versus L for $H=0.0$.

than the isolated-filament case. Besides, the flapping amplitude is greater, i.e., the effective projected area is bigger. Therefore the drag of the filament is increased compared to the uniform coming flow case. These combined may explain the results in Figs. 6(b) and (d).

Further, let us turn to the influence of vertical distance H on the drag coefficient C_D. Fig. 7 shows the C_D versus the H for three typical horizontal distance G for $L=1.0$ and 2.0. These plots show that the C_D of the cylinder is always reduced for all cases, but the C_D of the filament is reduced only for $L=1.0$ and it is increased for $L=2.0$ except for very small H in the $G=2.5$ case. As a consequence, the total C_D of the whole system is reduced only for $L=1.0$ and it is increased for $L=2.0$ except for small H and G. For both values of L, the function of C_D versus H is more complex when $G=2.5$ and becomes relatively simpler for greater values of G. Figs. 7(a), (b), (d) and (e) show that smaller values of G and H have more significant influence on the C_D of system; it means that the cylinder-filament-interaction is much more complicated when they are placed close to each other. This is probably due to the complex interaction of the flapping filament and the suction zone boundary.

From the preceding analysis, the C_D of the system depends on the filament length L. To reveal in detail how this parameter may influence the C_D, a series of simulations with varying L with $H=0.0$ and $G=5.0$ are performed. Fig. 8 plots the C_D of the cylinder and the C_D of the filament versus the filament length L. It is seen that the C_D of the cylinder is a monotonously decreasing function of L while the C_D of the filament is a monotonously increasing function of the L. This is to say that the drag coefficient of the cylinder is always reduced because of the presence of the filament and the greater the filament length L, the greater the reduction in C_D. For the drag coefficient of the filament, the outcomes depend on the filament length: small L induces drag reduction but large L induces drag increment.

4.3   Flapping frequency and amplitude of the filament

At the base values of all the parameters given at the beginning of this section, the dimensionless flapping frequency of the filament in a uniform flow is approximately 0.33; the
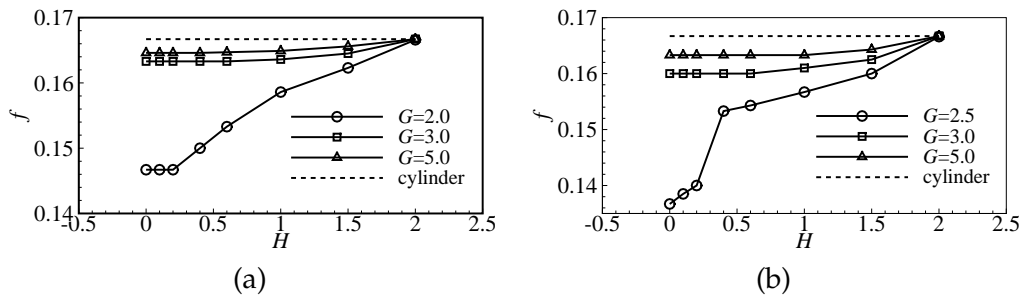
Figure 9: Frequency f of vortex shedding of the cylinder or the flapping of the filament versus H for for $L =$ (a) 1.0 and (b) 2.0.
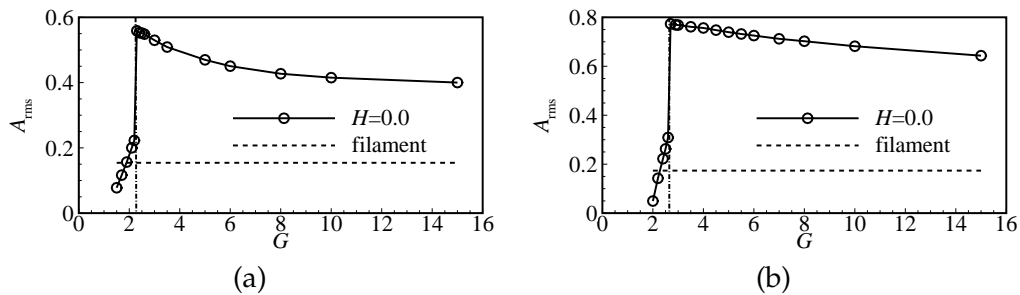

Figure 10: Root-mean-square value of the filament tail vertical position A_{rms} versus G for $L =$ (a) 1.0 and (b) 2.0.

vortex shedding frequency of the cylinder without the filament is approximately 0.166. When the two objects are placed in tandem in the same uniform flow, the frequency of the filament flapping becomes equal to the vortex shedding frequency of the cylinder because the filament is passive and compliant, and it simply oscillates with the wake of the cylinder. Fig. 9 shows the influence of vertical distance H on the frequency of the system for three typical values of G. It is seen that introduction of the trailing filament into the system causes the system frequency (i.e., vortex shedding and filament flapping) to decrease. The decrease is more pronounced for small values of G and H. Little change in the frequency is seen when the filament is horizontally or vertically placed far away from the cylinder.

The filament flapping amplitude A_{rms} is defined as the root mean square value of the vertical excursion of the filament free-end. Fig. 10 plots A_{rms} against the horizontal separation distance G for $H = 0.0$. The left panel corresponds to $L = 1.0$ and the right panel corresponds to $L = 2.0$. It is seen that when $G < G_c$, corresponding to RF state, the flapping amplitude is smaller than the filament-alone case because the filament vertical excursion is restricted to the suction zone; but when $G > G_c$, corresponding to NF state, it flaps outside of the suction zone and the free-end has no restrictions along the vertical direction except for the fixed-end. Thus the flapping amplitude is significantly increased compared to the filament-alone case. The increment is caused by the oscillating wake behind the cylinder which facilitates the filament flapping motion. Therefore the filament
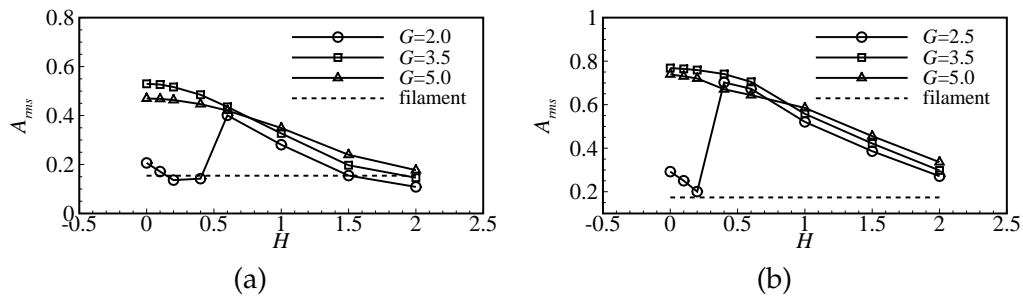
Figure 11: Root-mean-square value of the filament tail vertical position A_{rms} versus H for $L=$ (a) 1.0 and (b) 2.0.

flaps more violently with larger amplitude. The significant increase in A_{rms} by the wake is persistent with respect to separation distance and only slightly becomes smaller as G increases; the amplitude remains significantly greater than the filament-alone case even when the filament is placed far away from the cylinder (as far as $G=15.0$). This suggests filament flapping in the wake of an object is quite different from flapping in a uniform flow. Fig. 10 also shows that a longer filament has larger flapping amplitude in the wake of the cylinder.

To examine how the vertical separation distance H would influence the flapping amplitude, Fig. 11 shows the A_{rms} against H for three typical values of G for $L=1.0$ and 2.0. It is seen that if $G>G_c$, the amplitude is significantly increased, but quickly and monotonously approaches the filament-alone case as H increases; if $G<G_c$, the situation is more complicated because of filament-suction-zone-boundary interaction. This is probably caused by the fact that the filament is at RF state for smaller values of H and at NF state for greater values of H.

5   Concluding remarks

Numerical simulations are performed to understand the interaction of a upperstream rigid stationary cylinder and a downstream flexible flapping filament. Our simulations have identified two stable self-sustained flapping states of the filament: a normal flapping (NF) state where the filament flaps with the fixed-end upperstream and free-end downstream and a reversed flapping (RF) state where the filament flaps with the free-end upperstream and the fixed-end downstream. The reversed flapping is caused by the existence of the suction zone behind the cylinder and the critical horizontal cylinder-filament separation distance G_c depends on the Reynolds number and filament length. Our numerical results have found that the drag coefficient of the cylinder is always reduced by the presence of the downstream filament, but the drag coefficient of the filament is dependent on the filament length; it is reduced for sufficiently short filament in either flapping state and it may be decreased or increased dependent on the values of G and H for sufficiently long filament. For large value of G, the drag coefficient of the cylinder is a

monotonously decreasing function of the filament length while the drag coefficient of the filament is a monotonously increasing function of filament length L. Our computational studies have also shown that compared to the filament-alone case the filament's flapping frequency is decreased and its flapping amplitude is increased unless both G and H are very small.

The previous laboratory experiments showed that the drag of the trailing object is reduced in the case of two tandem rigid objects in a viscous flow, the drag of the leading object is reduced in the case of two tandem flexible objects. For the present case, the leading rigid cylinder experiences drag reduction, and the filament may experience drag increase or decrease dependent on the filament length. This indicates the inherit complexity of the fluid-structure-interaction. Furthermore, previous computational studies have shown that a massless filament does not possess a self-sustained flapping state in a uniform flow (i.e., no mass no flapping). However, in our case the filament is placed in the wake of a cylinder, and we find that a massless filament still has a self-sustained flapping state. This is because the trailing filament may simply oscillate with the oscillating wake behind the cylinder.

There are seven dimensionless parameters in our cylinder-filament-flow system: the Reynolds number Re, the filament mass density M, the filament bending modulus K_b and stretching coefficient K_s, the filament length L, the cylinder-filament horizontal and vertical separation distances G and H. For most of the simulations presented in this paper, the parameters Re, M, K_b and K_s are fixed. The Reynolds number has been varied to study the transition between the two flapping modes. Further, we will study the influence of these parameters on this system in the future.

Acknowledgments

References

[1] Z. XIA, K. W. CONNINGTON, S. RAPAKA, P. YUE, J. J. FENG, AND S. CHEN, *Flow patterns in the sedimentation of an elliptical particle*, J. Fluid Mech., 625 (2009), pp. 249–272.

[2] R. MITTAL, V. SESHADRI, AND H. S. UDAYKUMAR, *Flutter, tumble and vortex induced autorotation*, Theor. Comput. Fluid Dyn., 17 (2004), pp. 165–170.

[3] J. ZHANG, S. CHILDRESS, A. LIBCHABER, AND M. SHELLEY, *Flexible filaments in a fowing soap film as a model for one-dimensional flags in a two-dimensional wind*, Nature, 408 (2000), pp. 835–839.

[4] L. ZHU AND C. S. PESKIN, *Simulation of a flapping flexible filament in a flowing soap film by the immersed boundary method*, J. Comput. Phys., 179 (2002), pp. 452–468.

[5] J. LEE, J. SHIN AND S. LEE, *Fluid-structure interaction of a flapping flexible plate in quiescent fluid*, Comput. Fluids, 57 (2012), pp. 124–137.

[6] S. MICHELIN AND S. G. L. SMITH, *Resonance and propulsion performance of a heaving flexible wing*, Phys. Fluids, 21 (2009), pp. 071902.

[7] Y. SUI, X. B. CHEN, Y. T. CHEW, P. ROY AND H. T. LOW, *Numerical simulation of capsule deformation in simple shear flow*, Comput. Fluids, 39 (2010), pp. 242–250.

[8] Y. SUI, H. T. LOW, Y. T. CHEW AND P. ROY, *A front-tracking lattice Boltzmann method to study flow-induced deformation of three-dimensional capsules*, Comput. Fluids, 39 (2010), pp. 499–511.

[9] C.-K. KANG, H. AONO, C. E. S. CESNIK, AND W. SHYY, *Effects of flexibility on the aerodynamic performance of flapping wings*, J. Fluid Mech., 689 (2011), pp. 32–74.

[10] J. C. LIAO, D. N. BEAL, G. V. LAUDER, AND M. S. TRIANTAFYLLOU, *The Kármán gait: novel body kinematics of rainbow trout swimming in a vortex street*, J. Exp. Biol., 206 (2003), pp. 1059–1073.

[11] D. N. BEAL, F. S. HOVER, M. S. TRIANTAFYLLOU, J. C. LIAO, AND G. V. LAUDER, *Passive propulsion in vortex wakes*, J. Fluid Mech., 549 (2006), pp. 385–402.

[12] J. D. ELDREDGE AND D. PISANI, *Passive locomotion of a simple articulated fish-like system in the wake of an obstacle*, J. Fluid Mech., 607 (2008), pp. 279–288.

[13] Y. SUI, Y.-T. CHEW, P. ROY, AND H.-T. LOW, *A hybrid immersed-boundary and multi-block lattice boltzmann method for simulating fluid and moving-boundaries interactions*, Intl J. Numer. Meth. Fluids, 53 (2007), pp. 1727–1754.

[14] L.-B. JIA AND X.-Z. YIN, *Response modes of a flexible filament in the wake of a cylinder in a flowing soap film*, Phys. Fluids, 21 (2009), pp. 101704.

[15] S.-Y. WANG, L.-B. JIA, AND X.-Z. YIN, *Kinematics and forces of a flexible body in Kármán vortex street*, Chin. Sci. Bull., 54 (2009), pp. 556–561.

[16] F.-B. TIAN, H. LUO, L. ZHU, AND X.-Y. LU, *Interaction between a flexible filament and a downstream rigid body*, Phys. Rev. E, 82 (2010), pp. 026301.

[17] M. M. ZDRAVKOVICH, *Review of flow interference between two circular cylinders in various arrangement*, J. Fluids Eng., 99 (1977), pp. 618–633.

[18] L. RISTROPH AND J. ZHANG, *Anomalous hydrodynamic drafting of interacting flapping flags*, Phys. Rev. Lett., 101 (2008), pp. 194502.

[19] L. ZHU, *Interaction of two tandem deformable bodies in a viscous incompressible flow*, J. Fluid Mech., 635 (2009), pp. 455–475.

[20] F.-B. TIAN, H. LUO, L. ZHU, J. C. LIAO, AND X.-Y. LU, *An efficient immersed boundary-lattice Boltzmann method for the hydrodynamic interaction of elastic filaments*, J. Comput. Phys., 230 (2011), pp. 7266–7283.

[21] D. YU, R. MEI, AND W. SHYY, *A multi-block lattice Boltzmann method for viscous fluid flows*, Intl J. Numer. Meth. Fluids, 39 (2002), pp. 99–120.

[22] Y. KIM AND C. S. PESKIN, *Penalty immersed boundary method for an elastic boundary with mass*, Phys. Fluids, 19 (2007), pp. 053103.

[23] Z.-G. FENG AND E. E. MICHAELIDES, *Proteus: a direct forcing method in the simulations of particulate flows*, J. Comput. Phys., 202 (2005), pp. 20–51.

[24] F.-B. TIAN, H. LUO, L. ZHU, AND X.-Y. LU, *Coupling modes of three filaments in side-by-side arrangement*, Phys. Fluids, 23 (2011), pp. 111903.

[25] B. S. H. CONNELL AND D. K. P. YUE, *Flapping dynamics of a flag in a uniform stream*, J. Fluid Mech., 581 (2007), pp. 33–67.

[26] C. J. APELT, G. S. WEST AND A. A. SZEWCZYK, *The effects of wake splitter plates on the flow past a circular cylinder in the range $10^4 < Re < 5 \times 10^4$*, J. Fluid Mech., 61 (1973), pp. 187–198.